Molecular Diversity
https://doi.org/10.1007/s11030-019-10021-0

ORIGINAL ARTICLE

Identification and molecular modeling of new quinolin-2-one thiosemicarbazide scaffold with antimicrobial urease inhibitory activity

Mohammed A. I. Elbastawesy[1] · Yaseen A. M. M. El-Shaier[2] · Mohamed Ramadan[1] · Alan B. Brown[3] · Ashraf A. Aly[4] · Gamal El-Din A. Abuo-Rahma[5]

Received: 10 August 2019 / Accepted: 29 November 2019

Abstract

A new series of 6-substituted quinolin-2-one thiosemicarbazides **6a–j** has been synthesized. The structure of the target compounds was proved by different spectroscopic and elemental analyses. All the designed final compounds were evaluated for their in vitro activity against the urease-producing *R. mucilaginosa* and *Proteus mirabilis* bacteria as fungal and bacterial pathogens, respectively. Moreover, all compounds were in vitro tested as potential urease inhibitors using the cup-plate diffusion method. Compounds **6a** and **6b** were the most active with ($IC_{50} = 0.58 \pm 0.15$ and 0.43 ± 0.09 µM), respectively, in comparison with lead compound **I** ($IC_{50} = 1.13 \pm 0.00$ µM). Also, the designed compounds were docked into urease proteins (ID: 3LA4 and ID: 4UBP) using Open Eye® software to understand correctly about ligand–receptor interactions. The docking results revealed that the designed compounds can interact with the active site of the enzyme through multiple strong hydrogen bonds. Moreover, rapid overlay of chemical structures' analysis was described to understand the 3D QSAR of synthesized compounds as urease inhibitors. The results emphasize the importance of polar thiosemicarbazide directly linked to 6-substituted quinolone moieties as promising antimicrobial urease inhibitors.

✉ Ashraf A. Aly
ashrafaly63@yahoo.com

✉ Gamal El-Din A. Abuo-Rahma
gamal.aborahama@mu.edu.eg

[1] Department of Pharmaceutical Organic Chemistry, Faculty of Pharmacy, Al-Azhar University, Assiut 71524, Egypt

[2] Department of Organic and Medicinal Chemistry, Faculty of Pharmacy, University of Sadat City, Sadat-City, Menufia, Egypt

[3] Chemistry Department, Florida Institute of Technology, Melbourne, FL 32901, USA

[4] Department of Chemistry, Faculty of Science, Minia University, El-Minia 61519, Egypt

[5] Department of Medicinal Chemistry, Faculty of Pharmacy, Minia University, El-Minia 61519, Egypt

Published online: 08 January 2020

Graphic abstract

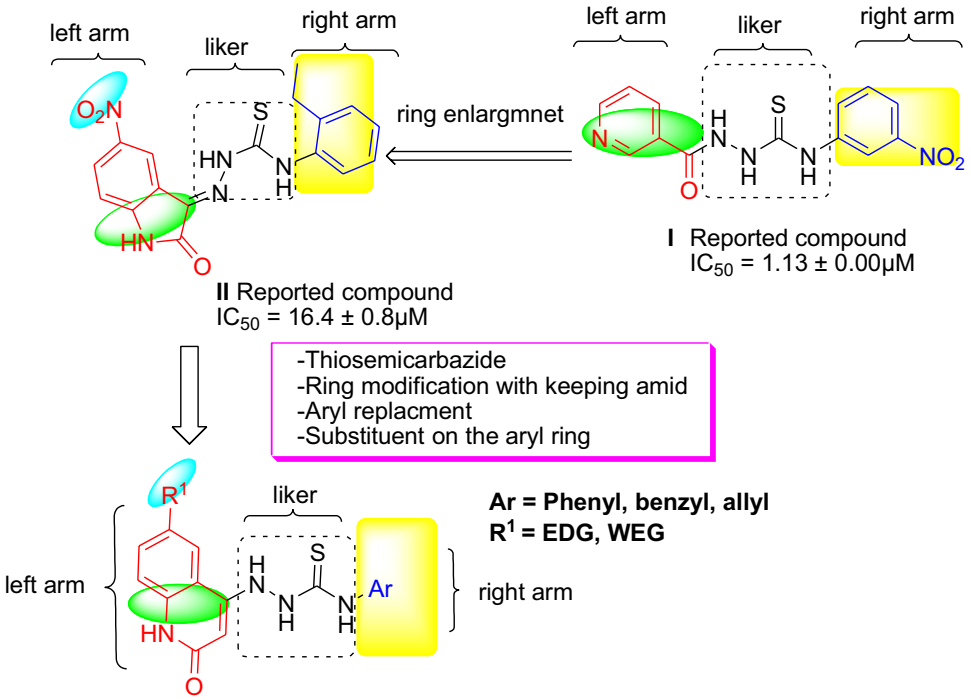

Keywords Molecular docking · ROCS analysis · *R. mucilaginosa* · *Proteus mirabilis* · Hybridization

Introduction

Nitrogen containing heterocycles are important structural units in medicinal chemistry. Among various heterocyclic compounds, quinolines have gained the largest attention. Throughout the twentieth century [1], the chemistry and biological applications of quinoline had been subjected to intense studies from different research groups [2]. On the other hand, urease (urea amidohydrolase, EC 3.5.1.5) is a famous nickel-containing metalloenzyme, which catalyzes the hydrolysis of urea into carbamate and ammonia [3]. Consequently, these reactions cause significant alkalinity due to the release of large quantities of ammonia. The increase in pH is directly associated with the development of numerous health complications in humans like kidney stone, hepatic coma and pyelonephritis which depend on colonization site by urease-producing microorganisms [4].

For example, *Rhodotorula* species uses urease enzyme as an essential factor for protection and spreading processes [5]. The most prevalent species is *R. mucilaginosa* which emerged as opportunistic pathogens with the ability to colonize and infect susceptible patients: Nearly 90% of patients with *R. mucilaginosa* infection have underlying solid or hematologic malignancy, organ/bone marrow transplant, or immunosuppression due to corticosteroid use, neutropenia or acquired immunodeficiency syndrome (AIDS) [6]. Moreover, *Proteus mirabilis*, a common cause of urinary tract infections (UTIs) in individuals with functional or structural abnormalities or with long-term catheterization, forms bladder and kidney stones as a consequence of urease-mediated urea hydrolysis [7], in addition to high and constant increase in antibiotic resistance [8, 9]. So, many researchers have been aiming for more targeted and safer therapy to kill or at least control these microbial infections for such complicated medical situations.

On a chemical front, thiosemicarbazides are a class of compounds, which has been found to possess a wide spectrum of biological properties [10] such as antitubercular [11], antiviral [12], herbicidal, antibacterial [13], antinociceptive [14] and antioxidant properties [15]. Recently, many studies have been reported on the efficacy of thiosemicarbazides and its hybrid derivatives to inhibit urease enzyme activity [4] (Fig. 1).

The application of chemical similarity analysis, either topological (2D) or superposition shape similarity (3D), in drug design is commonly used. It is a useful technique in drug discovery and drug design approaches. Shape similarity (3D) and electrostatic potential are considered as fundamental descriptors for computational drug discovery and understand correctly when we thinking about the protein ligand

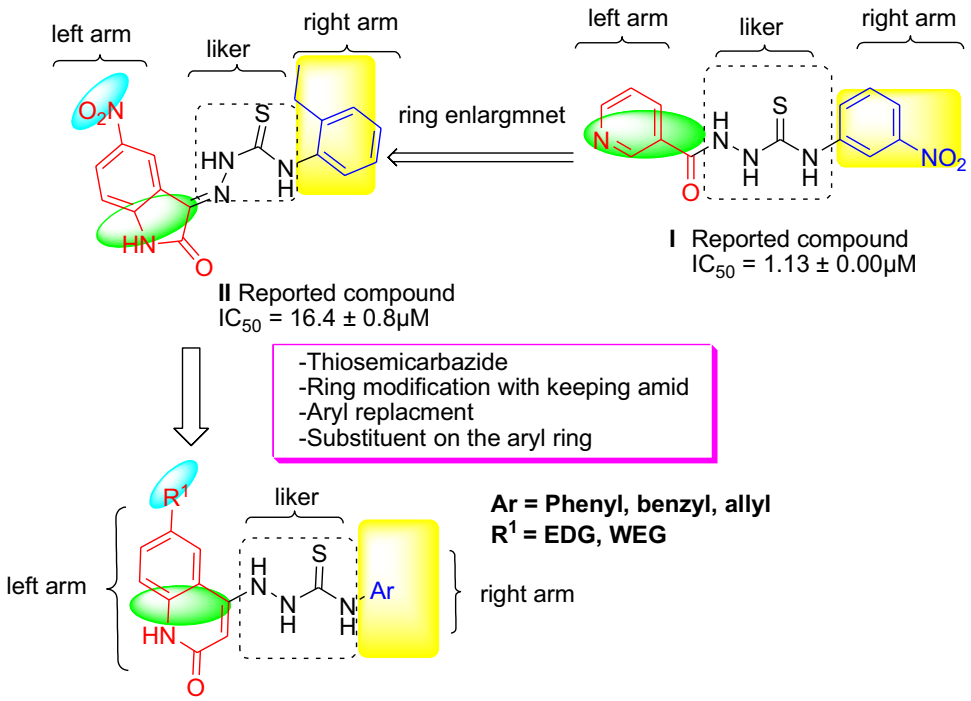

Fig. 1 Rationale for the design of the target compounds **6a–j**

binding. Shape similarity exhibits a good neighborhood behavior that high similarity in shape behaves reflective of high similarity in biology, while high similarity in biology is not reflected in the similarity in structure [16]. Shape similarity can be used in virtual screening [17], lead-hopping, molecular alignment, pose generation and predictions [18].

Based on the aforementioned information in the literature, and in continuation of our previous work in utilizing molecular modeling in drug design approaches [19–22] and in design of antibacterial urease inhibitors [23, 24], the aim of this research is to connect two well-known biologically active entities: quinolin-2-one with thiosemicarbazide scaffold for the purpose synergistic improvement for antimicrobial and/or urease inhibition activity for such different derivatives. The target compounds as depicted in Fig. 1 were designed, synthesized and subjected to molecular docking and ROCS technique [25] to calculate the shape similarity for our compounds to the reported standards and applied these descriptors to 3DQSAR study.

Results and discussion

Chemistry

The final target compounds **6a–j** were prepared as shown in Scheme 1. Compounds **2–5** were synthesized according to reported methods, and their structures were confirmed by matching their spectral data with the reported ones [26–28]. The key intermediates, hydrazine quinolones **5a–e,** were prepared by refluxing compounds **4a–e** with hydrazine hydrate for 12 h [22]. The final target thiosemicarbazides **6a–j** were prepared by reaction of the hydrazine derivatives **5a–e** and the appropriate isothiocyanate in dioxane under the reflux condition. The spectral and elemental data revealed that all derivatives **6a–j** underwent the reaction smoothly to give the respective thiosemicarbazide hybrid structure in good yield. The ^{1}H NMR spectra experienced the disappearance of NH_2 signal and appearance of four singlet (NH) signals at δ_H 7.89–11.24 ppm that augments the formation of thiosemicarbazide hybrids. As a representative example, ^{1}H NMR of compound **6e** showed singlet signals at δ_H 11.24, 9.99, 9.88, 9.24 ppm for four NH protons and also a characteristic pattern for the additional five phenyl protons at 7.16–7.42 ppm. Moreover, ^{13}C NMR spectrum showed the phenyl group: Four signals at δ_C 138.99, 127.90, 125.97 and 125.20 ppm represented mono-substituted phenyl. Further structural confirmation also was provided from the analysis of the ^{1}H-^{15}N HSQC spectrum of **6e**, which showed a broad singlet at δ_H 9.99, assigned as NH–Ph, and correlated with attached nitrogen which appears at δ_N 125.6. Also, ^{1}H NMR of compound **6i** showed a ddt J_d = 17.0, 9.8 Hz, J_t = 5.0 signal integrated with one proton at δ 5.35 ppm, another doublet at 4.55 with J = 11.0, in addition to another signal at 3.63 ppm J = 4.20 Hz, which was ascribed to the allyl moiety. ^{13}C NMR spectrum of the prepared final compounds showed the characteristic thioxo and ring oxo carbonyl groups at ~ δ 181.00 and 162.00 ppm, respectively. Furthermore, the mass spectra and elemental analyses data confirmed the structural formula.

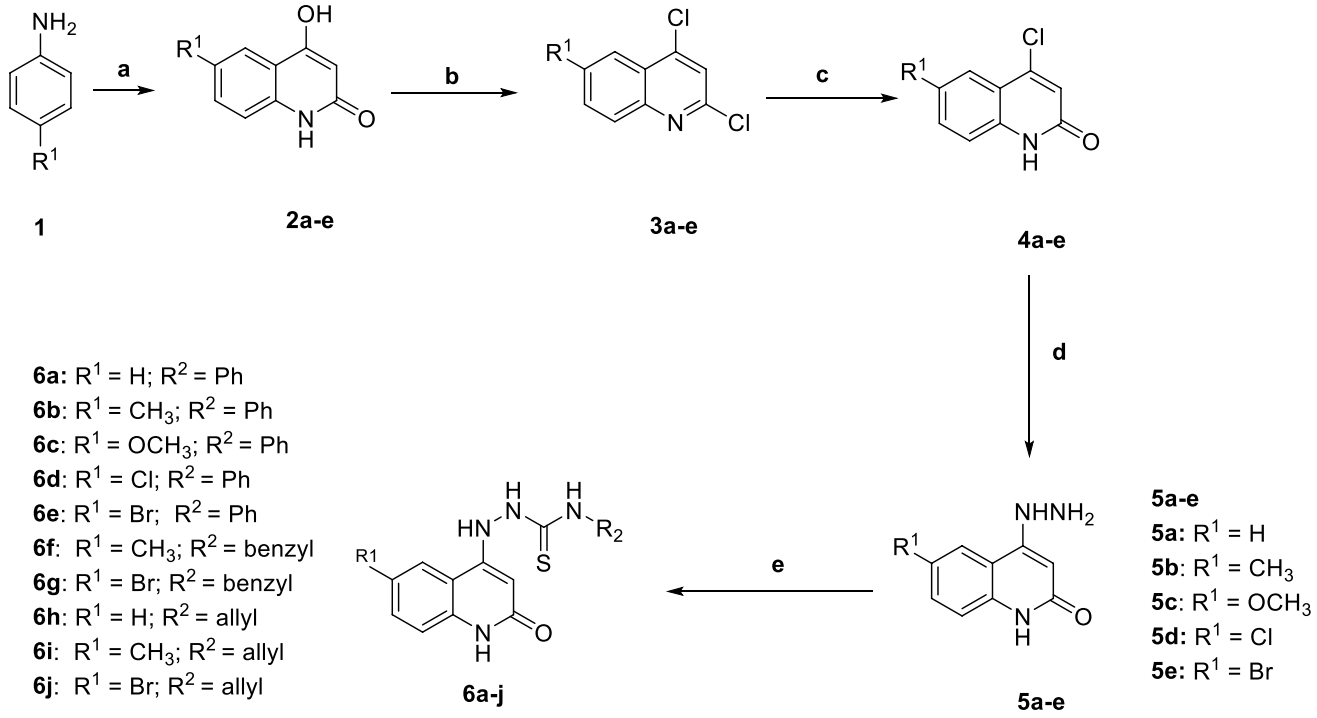

Scheme 1 Synthesis of target compounds **6a–j.** Reagent and reaction conditions: (a) diethyl malonate, PPA, reflux 3 h; (b) $POCl_3$, reflux 2 h; (c) AcOH, reflux 10 h; (d) $NH_2NH_2{\cdot}H_2O$ (85%), EtOH, reflux 8 h; (e) isothiocyanate derivatives, dioxane, reflux 3–4 h

Biology

Antifungal activity

All synthesized compounds were tested against the urease-producing *R. mucilaginosa* fungal strains using clotrimazole as a reference drug [29]. The results in Table 1 revealed that R. mucilaginosa show that the tested compounds have moderate-to-weak activity. Compounds **6d, 6f** and **6g** showed no activity against the tested fungal strains. On the other hand, compounds **6a, 6b, 6c, 6e, 6h, 6i** and **6j** showed approximate results of inhibition ranking from 48 to 56% from the

Table 1 Urease inhibition IC_{50} (μM), anti-*P. mirabilis* MIC (μM) and anti-*R. mucilaginosa* activity (inhibition zone in mm) of compounds **6a–j**

Comp.	IC_{50} (μM) Urease	MIC (μM) *P. mirabilis*	*Activity against R. mucilaginosa* (inhibition zone in mm)
6a	0.58 ± 0.15	661.7	12
6b	0.43 ± 0.09	669.1	13
6c	1.29 ± 0.36	762.5	13
6d	3.21 ± 0.27	732.3	NA
6e	9.45 ± 0.09	828.7	13
6f	5.80 ± 0.84	720.9	NA
6g	3.28 ± 0.10	857.2	NA
6h	6.80 ± 1.72	399.3	14
6i	2.29 ± 0.81	586.5	13
6j	1.98 ± 0.58	723	13
Thiourea	22.8 ± 1.31	–	–
Lead compound **I** [4]	1.13 ± 0.00	–	–
Lead compound **II** [4]	16.4 ± 0.8		–
Ciprofloxacin	–	1.26	–
Clotrimazole	–	–	25

NA no inhibition

activity of the reference clotrimazole. Compound **6h** was the most active one with 14-mm inhibition zone and better in activity, especially to its analogs **6i** and **6j**. Based on this finding, the nature of quinolone 6-substituent has no effect on the activity. Moreover, different substitutions on thiosemicarbazide moiety clearly changed the activity. Compounds **6a–e** with a terminal phenyl part showed 48–52% inhibition. However, compounds **6f** and **6g** with benzyl moiety showed no activity, and compounds **6h, 6i** and **6j** with allyl terminal part were the most active group, achieving 52–56% inhibitory activity.

Antibacterial screening

P. mirabilis strain was isolated from the urine of patients suffering from urinary tract infection. The strain was negative for hemolysis and motile and was urease positive. The test was done using the cup-plate diffusion method [30] (Table 1). The results indicated that the tested compounds are, in general, weakly or moderately active. Only one compound **6h**, out of the ten compounds tested, showed significant antibacterial activity against *P. mirabilis*. Overall, this compound proved to be the most active one. The findings also indicated that compounds **6a** and **6i** exhibited a promising antibacterial profile.

Urease inhibition activity

The new synthetic quinolone–thiosemicarbazide hybrids **6a–j** were further in vitro screened for their human urease inhibitory potential, using thiourea as a standard inhibitor [31]. The urease inhibitory activity and IC_{50} of the tested compounds at different concentrations were evaluated (Table 1). The results showed that all of the tested derivatives exhibited potential urease inhibitory activities ranking $IC_{50} = 0.43–9.45$ µM, exceeding the reference thiourea. Compounds **6a** and **6b** were the most active among the tested series: They inhibited the activity of the enzyme at all the tested concentrations achieving $IC_{50} = 0.58$ and 0.43 µM, respectively. Next to those, compounds **6e** and **6h** experienced comparably weaker activity with $IC_{50} = 9.45$ and 6.80 µM, respectively. Moreover, compounds **6c**, **6d**, **6f–i** and **6j** were found to exhibit varying degrees of inhibitory effect at one or more tested concentrations. Overall, compounds **6a** and **6b** with a thiosemicarbazide phenyl terminal were proved to be the most potent inhibitors in the present series, as they exhibited relatively much greater activity with approximately 50-fold more potent than thiourea at a greater number of tested concentrations.

Ureases obtained from different sources contain (in addition to the nickel metal) one to three protein subunits present in varying stoichiometric ratios. A urease inhibitor can, therefore, interact either with the metal or the protein component to interfere with the enzymatic activity. A wide variety of mechanisms including un-competitive, competitive, non-competitive or even cooperative binding are known to be involved in the interaction of an inhibitor with an enzyme. Although the exact mechanism of urease inhibition by our test series **6a–j** is not fully known or investigated, but rather than the ordinary chelating mechanism (which reported for thiourea on the enzyme Ni part), we believe that the presence of quinolone part in our designed compounds gives them opportunity to inhibit the enzyme in such different ways. Furthermore, since the usual average plasma concentration of any drug is about 5 µg/mL [32], the anti-urease target compounds are considered potential candidates as a leading compound for further investigation.

Molecular modeling

Docking study

Urease is secreted by a diverse of bacterial species, either normal flora or pathogens. It is considered as a potent virulence factor and in metabolism for some bacteria as *Proteus mirabilis* and *Helicobacter pylori* [33]. Urease is necessary for its colonization of the gastric mucosa [34]. All of the target compounds have IC_{50}% better than lead **II,** and compounds **6a** and **6b** are better than lead **I**. Our hypothesis was directed to examine the binding mode and the pharmacophoric features of our designed scaffold utilizing docking and shape similarity studies using known compound **I** and compound **II** [4], as shown in Fig. 1, as lead standards.

The docking studies for the synthesized compounds were operated on the basis of crystal structures of urease proteins (ID: 3LA4 and ID: 4UBP) using Open Eye® software [35–37]. Open Eye Omega application was used to generate different conformations of each ligand. Docking was conducted using Fred, and the data were visualized by Veda application. This software package generates consensus scoring, which is a filtering process to obtain virtual binding affinity; the lower consensus score means a better binding affinity of the ligands toward the receptor. The compounds are ranked according to their consensus score, as given in Table 2. Interestingly, the consensus score values for the tested compounds are almost in parallel with IC_{50} values.

Docking with 3LA4 Furthermore, docking of compound **I** with 3LA4 [38] receptor revealed a consensus score of 79. It forms different hydrogen bonding (HB) interactions (as acceptor) with polar amino acids in the receptor cleft (as donor). The left arm constitutes this compound bound to Arg 609: A with HB (length 3.14 Å) through the nitrogen of pyridine ring. The right arm forms HB with Met 737A (length 2.37 Å) through the nitro group. The polar thiosemicarbazide linker interacts with the formation of two HBs

Table 2 Molecular modeling consensus scores of compounds **6a**, **6b** and lead compounds **I and II**

Compound	Consensus score	
	3LA4	4UBP
Compound **I**	79	97
Compound **II**	80	95
6a	84	96
6b	45	65

with Arg 439 (length 3.20 Å and 3.02 Å) through the sulfur atom (Fig. 2a). Compound **II** docked with consensus score 80. The NH of indole moiety (left arm) incorporated in HB with His 593: A with the length of 2.30 Å. The linker forms two HBs with Arg 439: A-alan 440: A through the sulfur atom and NHNH C=S of the thiosemicarbazide functionality with lengths of 3.19 Å and 1.83 Å, respectively (Fig. 2b). Then, the study was directed to understand our compounds' interaction. Compound **6b**, the most potent among the synthesized compounds, interacts with good interaction than the lead **I** and lead **II** with consensus score 45 through the formation of hydrophobic–hydrophobic interactions only (no HBs formation) as shown in Fig. 2c. All of its pharmacophoric features (right arm, linker and left arm) occupy the receptor clefts as lead compounds **I** and **II** and showed best overlay to these leads (Fig. 2d).

Compound **6a** docked with the target receptor with consensus score 84 and with different poses because its left and right arms bound the receptor clefts in a reverse pattern to standards **I** and **II** and compound **6b** (Fig. 2e). The carbonyl of quinolone-one motif (left arm) forms two HBs with the amino acid Arg: 439A (length 2.99 and 2.51 Å). This amino acid interacted with polar linker in case of compounds **I** and **II**. The internal nitrogen of the linker NHNH C=SNH thiosemicarbazide functionality forms HB with CME 592: A (length 2.29 Å).

Docking with 4UBP Docking was then carried out on 4UBP protein [39]. The receptor of this enzyme contains two pockets linked together. Compound **I** docked with the receptor (with consensus score 97) by formation of two HBs with Ala: 366A through the NH of the polar linker NHNH C=SNH as donor and HB with Gly 368C: A through the N of pyridine moiety (left arm) as acceptor. The nitrophenyl moiety (right arm) adopted the receptor pocket in a hydrophobic–hydrophobic interaction (Fig. 3a). Compound **II** docked in the receptor in one pocket without interaction to other sites with consensus score 95. It forms HB with Asp 224C: A through the internal of NHNH C=SNH (length 1.54 Å) as donor. Both the indole and phenyl moieties docked through hydrophobic–hydrophobic interactions (Fig. 3b).

Compound **6b,** the most potent among the synthesized compounds, binds the receptor in one pocket of receptor as compound **II** with the best consensus score of 65. Compound **6b** interacts through the formation of two HBs with Lys: 169C A through the two terminals NHNH C=SNH to form a cyclic form (Fig. 3c) (lengths 2.46 Å and 1.37 Å, respectively). Also, the internal NH of thiosemicarbazide functionality NHNH C=SNH forms HB with Meth: 367C A (length 1.48 Å). The quinolone moiety, which represents the right arm, adopted the receptor pocket and formed two HBs with Hist: 323C A and Arg: 339 C A through the amide functionality. The right arm lays in the receptor with hydrophobic–hydrophobic interactions (Fig. 3c). Compound **6a** interacts with the receptor with consensus score 96. It forms two HBs with Asp: 224C A through the two terminals of the linker NHNH C=SNH (lengths 1.93 Å and 1.91 Å). The NH of quinolone moiety forms HB with Ala 366: A (length 2.12 Å), as shown in Fig. 3d. However, both compounds **6a** and **6b** form HB with Ala: 366 A, but with a different pose inside the receptor. This behavior emphasizes the role of methyl substituent in quinolinyl moiety.

ROCS analysis and 3DQSAR

3D shape-based superposition (ROCS) is a method that used to predict similarity between compounds based on their three dimensional. ROCS alignment requires: (a) query molecules and those queries should be the standard or lead compounds, here are compounds **I** and **II**, as given in Table 2 and (b) the database molecules that our designed compounds. The outputs from ROC analysis are the overlay between the query and database molecules as visualized by vROCS and VIDA applications. The visualization of the query includes shape counter, shape atoms and color atom labels. The color shape of query compound **I**, illustrated in the following atoms, labels 2 rings, 3 donors, and 5 acceptors (Fig. 4a). The color shape of query compound **II** illustrated 3 rings, 5 donors, 4 acceptor and hydrophobic sites (Fig. 5a). Compounds **6a** and **6b** showed overlay with query **I**, as represented in Fig. 4b, c, respectively. Even the query represented extra donor and acceptor sites to the most active compounds **6a** and **6b**, and compound 6b represented high similarity to color atom of query **I** (Fig. 4c) than that obtained by **6a**, as shown in Fig. 4b, and compounds **6a** and **6b** adopted different shape atoms to query **I** (Fig. 4c). This pattern is due to the presence of methyl group in position 6 of quinolone ring.

In consideration of lead **II** as a query, both compounds **6a** and **6b** adopt high overlay to color atoms of the left atom (indole moiety) and polar linker (thiosemicarbazide functionality). The two compounds fail to adopt color atom of the left arm of query **II** (Fig. 5b), while both compounds **6a** and **6b** exhibited similar alignment in shape atoms to query **II** (Fig. 5c).

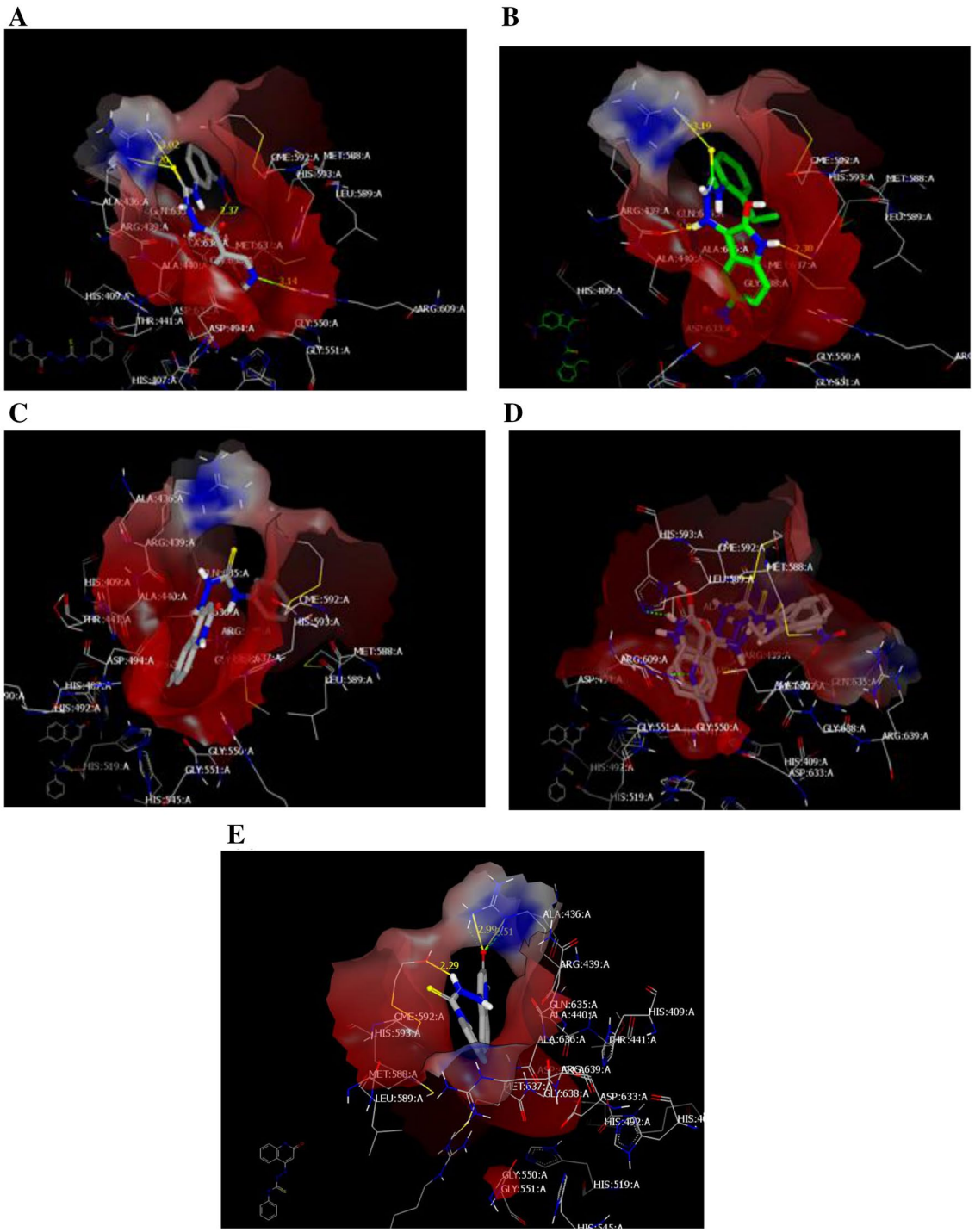

Fig. 2 Visual representation for **a** standard **I**; **b** standard **II**; **c** compound **6b**; and **d** overlay of the binding modes of **6b** and standards **I** and **II** docked with PDB ID: **3LA4**; **e** compound **6a** forms HB with essential amino acids. These compounds illustrated HB (dashed green lines) and hydrophobic–hydrophobic interaction toward urease-binding site (PDB ID: **3LA4**). (Color figure online)

Finally, we subjected the most active compounds **6b** to ROCS as a query. Compound **6b** showed atoms labels: 3 rings, 4 donors and 2 acceptors (Fig. 6a).

The second output of ROCs analysis is the score. Score represents various aspects of that alignment. The two core scoring methods are Shape Tanimoto (Tanimoto coefficient) and Color Tanimoto. Tanimoto Combo is the sum of those

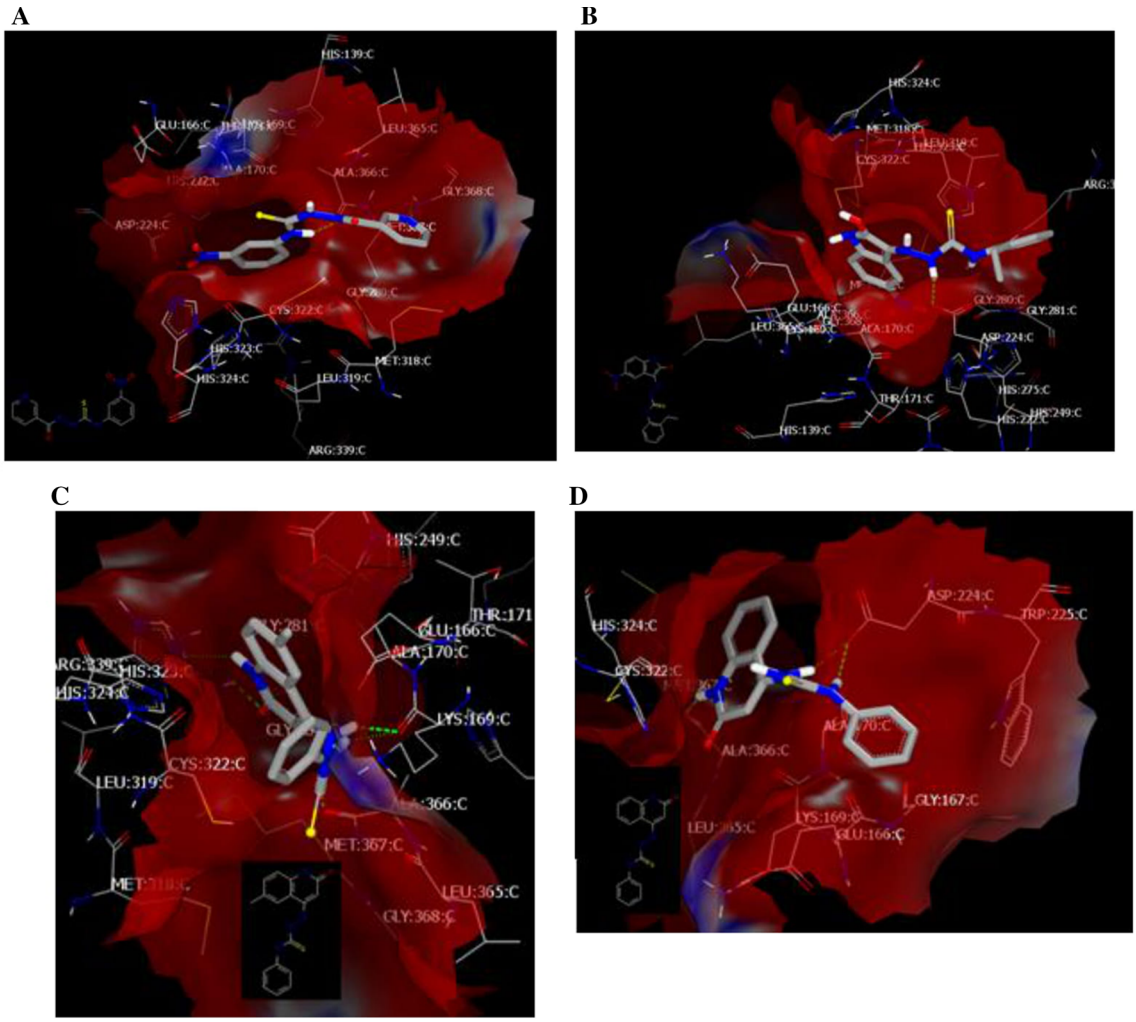

Fig. 3 Visual representation for **a** standard **I**, **b** standard **II**, **c** compound **6b**, **d** compound **6a** forms HB with essential amino acids in a different pose. These compounds illustrated HB (dashed green lines) and hydrophobic–hydrophobic interaction toward urease-binding site (PDB ID: **4UBP**). (Color figure online)

two independent components (Shape and Color Tanimoto). Shape Tanimoto represents the shared volume and mismatch volume and has scale from 0 to 1. Color Tanimoto is the distribution of chemical features in 3D (also scale from 0 to 1) (Table 3). The scores are computed, and the process is repeated to each conformation of the query molecules (**I** and **II**) and each conformation for the database molecules **6a–e** (Table 3). All compounds showed higher score in Tanimoto combo to lead **II** (as query) in the range from 1.24 to 1.01 rather than the lead **I** (as query) in the range from 1.05 to 0.92.

By studying the Tanimoto scores values, we found that compounds score Tanimoto Color descriptor is best-matched with compounds' activity rather than the summation descriptor (Tanimoto Combo). Considering lead **II** as query, compounds were **6c > 6d = 6b = 6a > 6e**. Regarding lead **I** as a query, the Tanimoto colors similarity of compounds was **6c > 6a = 6b > 6i > 6g = lead II**. This ranking indicating the right arm is essential to be aryl directly attached to the polar thiosemicarbazide linker.

From previous data, the synthesized compounds ranked best which need not to be structurally similar (in a 2-D sense) to the queries. In this study, our designed compounds are more similar to lead **II** as shown in number of atom labels (Fig. 6a), and shape similarity using Tanimoto Color is a good descriptor in the expected **3DQSAR** determination. In order to understand the 3D pharmacophoric feature of our compounds and figure out their 3DQSAR, ROCS was operated with compound **6f**, and we can find from the figure that the compound does not exhibit complete overlay with query **II**. The benzyl arm adopted perpendicular position of the phenyl group in

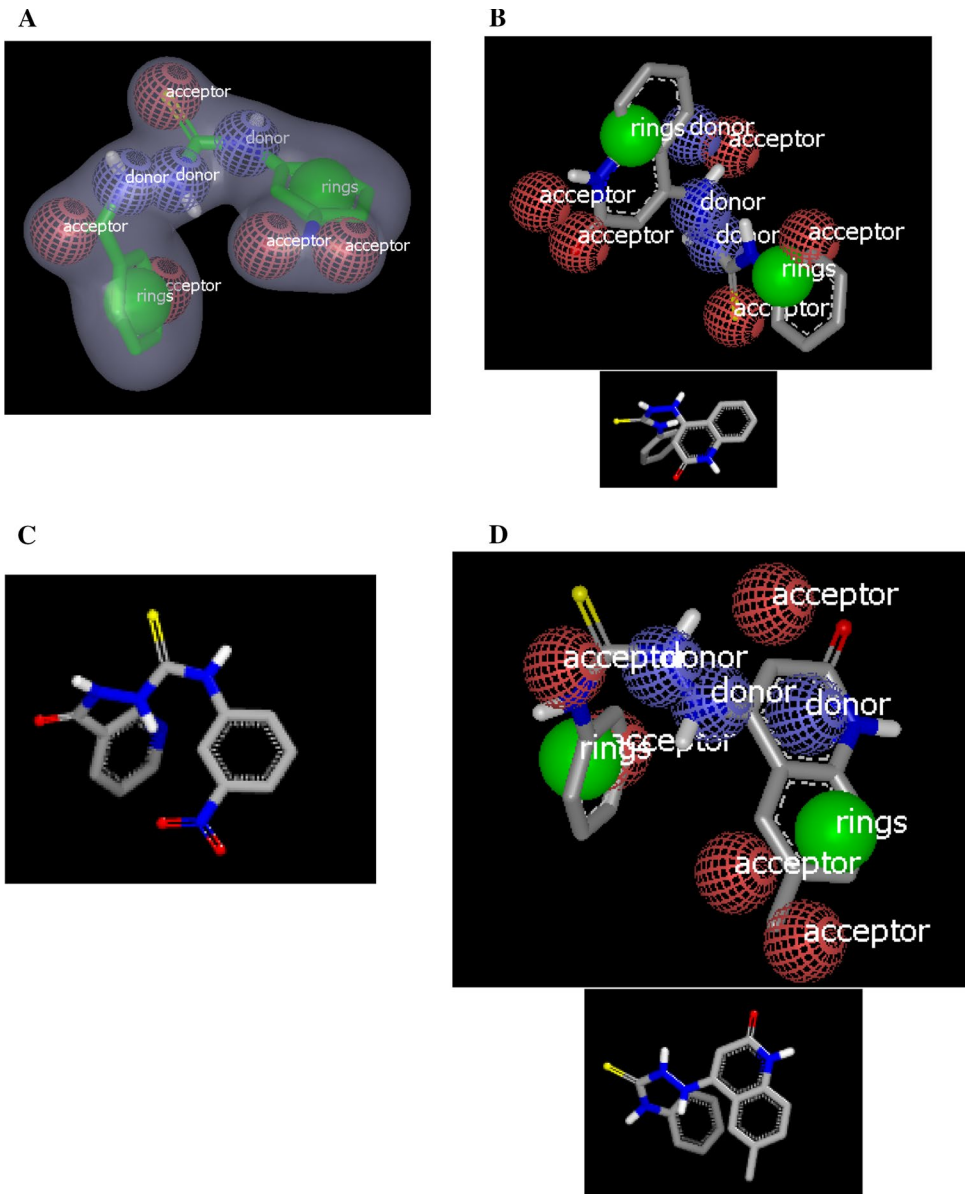

Fig. 4 **a** Representation of shape and color atoms of compound **I** as query by vROCS application; **b** overlay and alignment of **6a** on compound **I** shape; **c** overlay and alignment of **6b** on compound **I** shape. Both compounds **6a** and **6b** show dissimilarity in quinolone ring to query **I**

lead **II**, and its quinolone moiety does not overlay with the indole moiety (Fig. 5a–c). According to these findings, the presence of phenyl group in the thiosemicarbazide terminal is also important. The cyclic amide in quinolone system participates in formation of HB with essential amino acids inside the receptor. Also, 2D structure is not essential and 3D is more accurate which is represented by Tanimoto Color. These findings will guide us in the future, to elaborate new urease inhibitors originated from different scaffold systems by keeping the essential pharmacophoric features.

Conclusion

A new series of quinolin-2-one thiosemicarbazide derivatives **6a–j** have been synthesized and characterized by different spectroscopic and elemental analysis techniques including ^{1}H NMR, ^{13}C NMR, 2D NMR, MS and elemental microanalyses. In vitro screening of antimicrobial activity was carried out for all the synthesized compounds against the urease-producing *R. mucilaginosa* and *Proteus mirabilis* strains. Results revealed that most of the tested compounds showed moderate-to-good activity

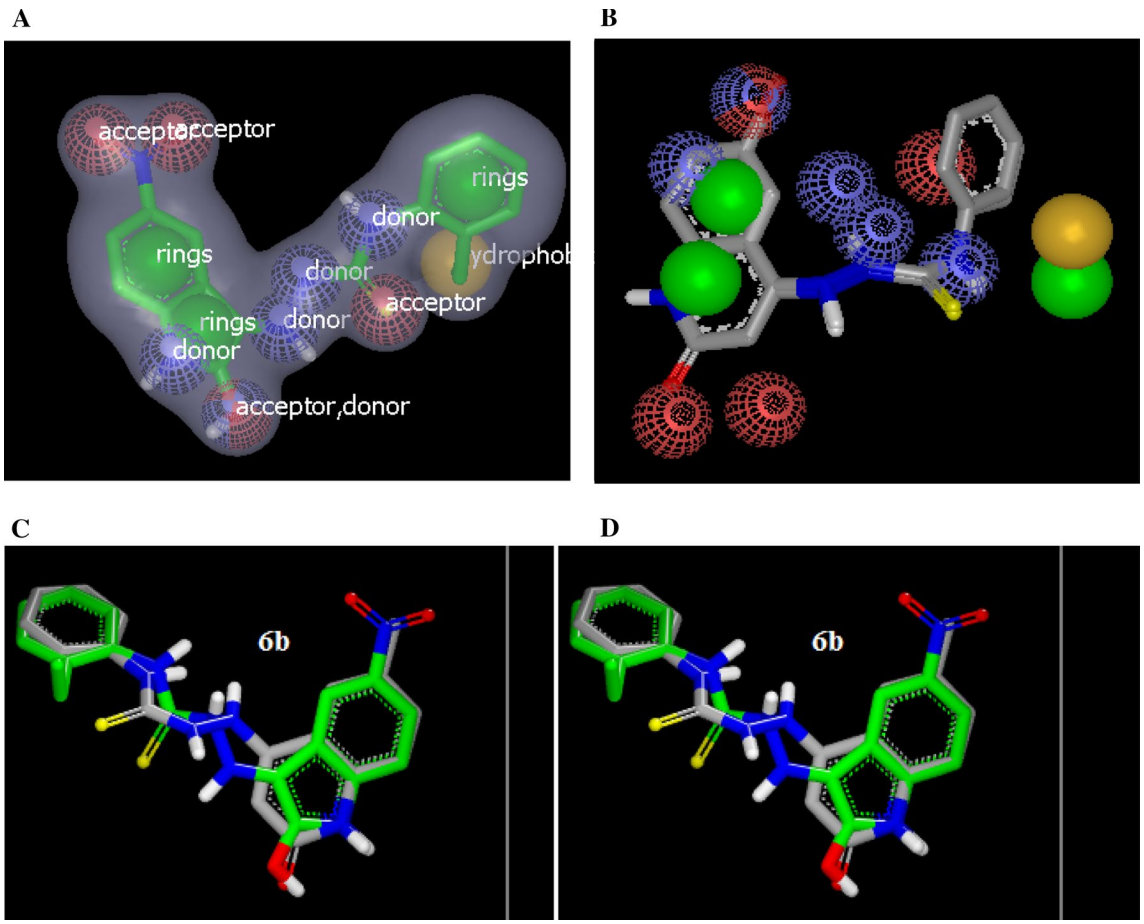

Fig. 5 **a** Representation of shape and color atoms of compound **II** as query by vROCS application; **b** overlay and alignment of **6a** and **6b** on compound **II** shape; **c** both compounds **6a** and **6b** show similarity in color and shape to lead **II**

against *R. mucilaginosa*, with 12–14 mm zone of inhibition compared to clotrimazole (25 mm). Compound **6h** experienced the highest anti-*P. mirabilis* activity achieving MIC = 399.3 µM which represents about 300 times less activity than the reference ciprofloxacin. Moreover, all the prepared compounds were in vitro tested as potential urease inhibitors. Among the tested compounds, **6a** and **6b** were the most active, showing a potent urease inhibition activity on different tested concentrations ($IC_{50} = 0.58 \pm 0.15$ and 0.43 ± 0.09 µM) and proved that they could be potential candidates for further investigation to treat certain clinical conditions caused by microbial ureases. Molecular docking showed the importance of thiosemicarbazide as a rich donor and acceptor. Quinolone system contains amide part (donor and acceptor also) to from HB. The use of ROCS led to the identification of a new inhibitor with diverse scaffolds presenting synthetic opportunities. The scaffolds should contain polar linker rich with donor and acceptor pharmacophore and linked directly with two aryl systems; the aryl should contain 1 or 2 rings and contain donor and acceptor pharmacophore parts. To the best of our knowledge, this is the first example of inhibition of this enzyme by quinolone-derived thiosemicarbazides. The present study provides a knowledge that encourages researchers for further modification of this scaffold to be more active antibacterial and/antifungal urease inhibitors.

Experimental

Chemistry

Reagent and materials

Unless otherwise noted, all materials were obtained from commercial suppliers and used without further purification. Reactions were monitored by TLC (Kieselgel 60 F_{254} precoated plates, E-Merck, Germany); the spots were detected by exposure to UV lamp at 254 nm. Melting points were determined on an electrothermal melting point apparatus (Stuart Scientific Co.) and were uncorrected. NMR spectra

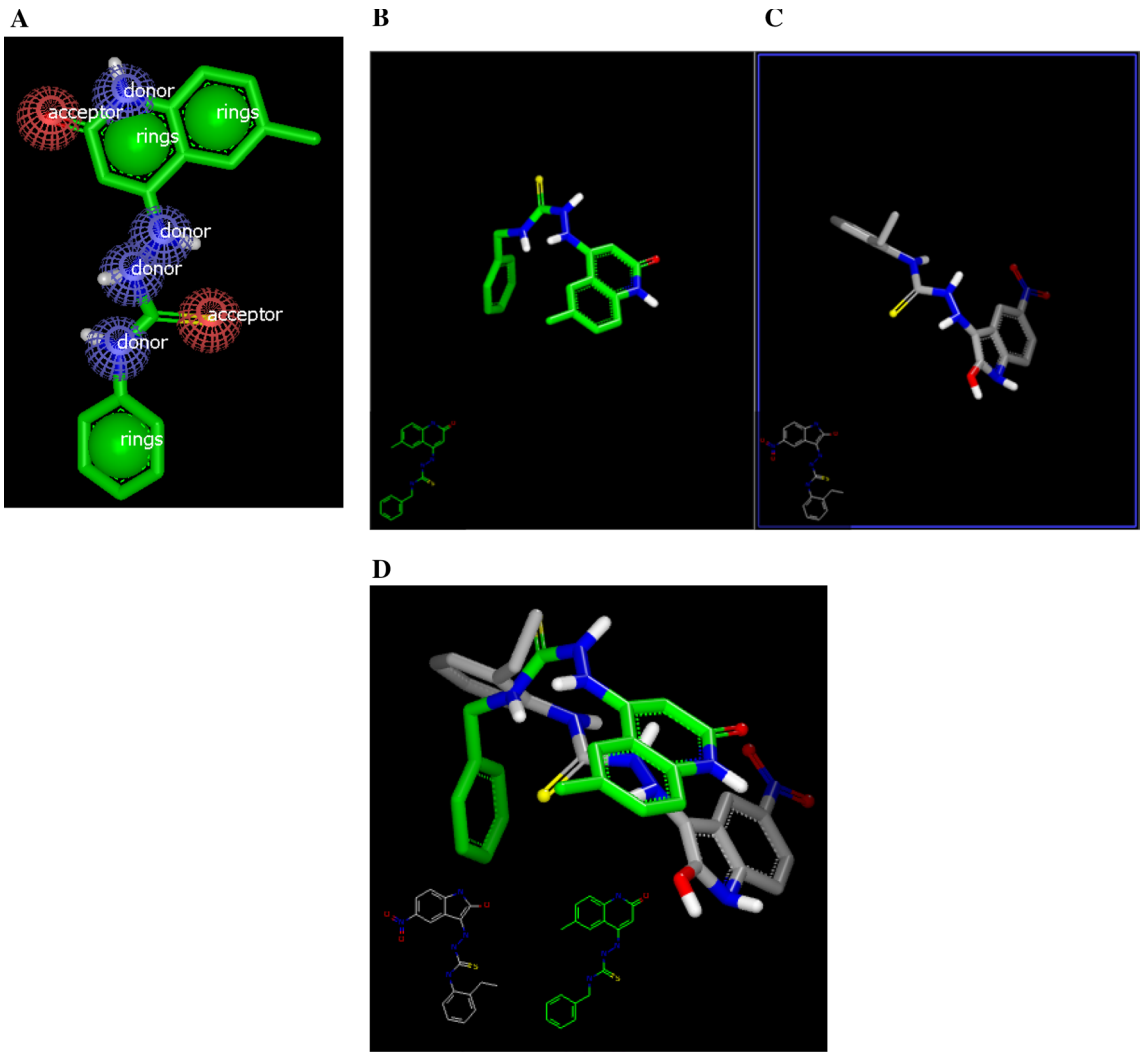

Fig. 6 **a** Representation of shape and color atoms of compound **6b** as query by vROCS application**; b** 3D visual representation of compound **6f**; **c** 3D visual representation of lead **II**; **D)** visual representation of compound **6f** and lead **II** and showed dissimilarity

Table 3 Tanimoto scores for compounds **6a–j** and lead compounds **I** and **II** as query

Compd.	Tanimoto Combo (Stand I as query)			Tanimoto Combo (Stand II as query)		
		Shape Tanimoto	Color Tanimoto		Shape Tanimoto	Color Tanimoto
6c	1.02	0.72	0.30	1.24	0.83	0.41
6a	0.98	0.71	0.27	1.17	0.77	0.39
6b	0.93	0.72	0.27	1.21	0.81	0.39
6i	0.94	0.68	0.26	1.03	0.83	0.30
6g	1.03	0.78	0.25	1.07	0.75	0.31
Lead **II**	0.96	0.71	0.25	2.00	1	1
6d	1.02	0.78	0.24	1.21	0.81	0.39
6j	0.93	0.69	0.24	1.01	0.73	0.28
6h	0.92	0.68	0.24	1.00	0.72	0.28
6f	1.05	0.7	0.21	1.08	0.76	0.33
6e	0.92	0.72	0.20	1.19	0.81	0.37
Lead **I**	2	1	1	1.01	0.72	0.28

were measured on a Bruker AV-400 spectrometer (Bruker BioSpin Corp., Billerica, MA, USA) (400 MHz for ^{1}H, 101 MHz for ^{13}C and 40.55 MHz for ^{15}N) at Florida Institute of Technology, USA. The ^{1}H and ^{13}C-NMR chemical shifts are given relative to internal standard TMS = 0; ^{15}N shifts are reported versus external neat nitromethane = 0. Vario EL III German CHN Elemental analyzer model was used for elemental analysis. Preparation and analytical data of compounds **2–5** were as reported [22].

General procedure for the synthesis of compounds 6a–j

To a suspension of hydrazinoquinoline **5** (1 mmol) in dioxane (25 mL), the appropriate isothiocyanate derivatives (1 mmol) were added and the mixture was heated at reflux on a boiling water bath for 3–4 h. The mixture was then left to cool, and the precipitate so formed was collected by filtration, washed with methanol and recrystallized by ethanol to give the target compounds.

2-(2-Oxo-1,2-dihydroquinolin-4-yl)-*N*-phenylhydrazinecarbothioamide (6a) Yield: 0.23 g (74%); mp: 185–187 °C, ^{1}H NMR (400 MHz, DMSO-d_6) δ ppm 11.00 (s, 1H, –CO–NH), 9.92 (s, 1H, Ar–NH), 9.84 (s, 1H, quin-NH), 9.15 (s, 1H, NNH), 7.77 (d, J = 8.0 Hz, 1H, quin-Ar–H), 7.46–7.41 (m, 3H, quin-Ar–H), 7.30–7.14 (m, 5H, Ar–H), 5.51 (s, 1H, C=CH). GS MS: m/z calcd: 310.09, found: 310.20. Anal. Calcd for $C_{16}H_{14}N_4OS$ (310.09): C, 61.92; H, 4.55; N, 18.0. Found: C, 61.79; H, 4.35; N, 17.90.

2-(6-Methyl-2-oxo-1,2-dihydroquinolin-4-yl)-*N*-phenylhydrazinecarbothioamide (6b) Yield: 0.29 g (91%); mp: 215–217 °C, ^{1}H NMR (400 MHz, DMSO-d_6) δ ppm 11.03 (s, 1H, –CO–NH), 9.94 (s, 1H, Ar–NH), 9.86 (s, 1H, quin-NH), 9.15 (s, 1H, NNH), 7.77 (s, 1H, quin-Ar–H), 7.44 (d, J = 7.6 Hz, 2H, Ar–H), 7.33 (d, J = 7.8 Hz, 1H, quin-Ar–H), 7.32 (t, J = 7.9 Hz, 2H, Ar–H), 7.17 (d, J = 8.4 Hz, 1H, quin-Ar–H), 7.16 (t, J = 7.3 Hz, 1H, Ar–H), 5.50 (s, 1H, = CH), 2.35 (s, 3H, CH_3).^{13}C NMR (101.0 MHz, DMSO-d_6) δ ppm 181.07, 162.73, 151.46, 139.06, 137.03, 131.47, 129.29, 127.85, 125.88, 125.10, 122.63, 115.26, 112.14, 93.70, 20.65. GS MS: m/z calcd: 324.10, found: 324.86. Anal. Calcd for $C_{17}H_{16}N_4OS$ (324.10): C, 62.94; H, 4.97; N, 17.27. Found: C, 62.53; H, 4.74; N, 17.03.

2-(6-Methoxy-2-oxo-1,2-dihydroquinolin-4-yl)-N-phenylhydrazine-carbothioamide (6c) Yield: 0.28 g (83%); mp: 200–202 °C, ^{1}H NMR (400 MHz, DMSO-d_6) δ ppm 11.00 (s, 1H, –CO–NH), 9.95 (s, 1H, Ar–NH), 9.88 (s, 1H, quin-NH), 9.15 (s, 1H, NNH), 7.47 (s, 1H, quin-Ar–H), 7.41 (d, J = 7.4 Hz, 2H, Ar–H), 7.31 (m, 2H, quin-Ar–H), 7.21–7.14 (m, 3H, Ar–H), 5.50 (s, 1H, = CH), 3.79 (s, 3H, OCH_3).^{13}C NMR (101.0 MHz, DMSO-d_6) δ ppm 181.11, 162.46, 153.43, 151.38, 139.04, 133.48, 127.87, 125.95, 125.16, 119.33, 116.58, 112.63, 105.40, 94.07, 55.63. GS MS: m/z calcd: 340.10, found: 340.41. Anal. Calcd for $C_{17}H_{16}N_4O_2S$ (340.10): C, 59.98; H, 4.74; N, 16.46. Found: C, 59.70; H, 4.56; N, 16.73.

2-(6-Chloro-2-oxo-1,2-dihydroquinolin-4-yl)-N-phenylhydrazinecarbothioamide (6d) Yield: 0.28 gm, (81%; mp: 224–226 °C, ^{1}H NMR (400 MHz, DMSO-d_6) δ ppm 11.26 (s, 1H, –CO–NH), 9.99 (s, 1H, Ar–NH), 9.90 (s, 1H, quin-NH), 9.29 (s, 1H, NNH), 8.04 (s, 1H, quin-Ar–H), 7.55 (d, J = 7.1, 1H, quin-Ar–H), 7.42 (d, J = 6.9, 2H, Ar–H), 7.32 (t, J = 7.2 Hz, 2H, Ar–H), 7.28 (d, J = 9.1, 1H, quin-Ar–H), 7.16 (t, J = 7.1, 1H, Ar–H), 5.54 (s, 1H, CH). GS MS: m/z calcd: 344.05, found: 344.23. Anal. Calcd for $C_{16}H_{13}ClN_4OS$ (344.05):C, 55.73; H, 3.80;N, 16.25. Found: C, 55.92; H, 3.57; N, 16.49.

2-(6-Bromo-2-oxo-1,2-dihydroquinolin-4-yl)-N-phenylhydrazinecarbothioamide (6e) Yield: 0.32 g (82%); mp: 230–232 °C, ^{1}H NMR (400 MHz, DMSO-d_6) δ ppm 11.24 (s, 1H, –CO–NH), 9.99 (s, 1H, Ar–NH), 9.88 (s, 1H, quin-NH), 9.28 (s, 1H, NNH), 8.17 (s, 1H, quin-Ar–H), 7.65 (dd, J = 8.8, 2.0, 1H, quin-Ar–H), 7.42 (d, J = 7.7, 2H, Ar–H), 7.32 (t, J = 7.8, 2H, Ar–H), 7.22 (d, J = 8.8, 1H, quin-Ar–H), 7.16 (t, J = 7.3, 1H, Ar–H), 5.53 (s, 1H,, = CH).^{13}C NMR (101.0 MHz, DMSO-d_6) δ ppm 181.02, 162.57, 150.72, 138.99, 138.13, 132.98, 127.90, 125.97, 125.60, 125.20, 117.43, 113.97, 112.47, 94.21. GS MS: m/z calcd: 388.00, found: 388.22. Anal. Calcd for $C_{16}H_{13}BrN_4OS$ (388.00): C, 49.37; H, 3.37; N, 14.39. Found: C, 49.40; H, 3.31; N, 14.46.

***N*-Benzyl-2-(6-methyl-2-oxo-1,2-dihydroquinolin-4-yl) hydrazinecarbothioamide (6f)** Yield: 0.26 g (77%); mp: 239–240 °C, ^{1}H NMR (400 MHz, DMSO-d_6) δ ppm 11.00 (s, 1H, –CO–NH), 9.61 (s, 1H, CH_2-NH), 9.03 (s, 1H, quin-NH), 8.83 (s, 1H, NNH), 7.74 (s, 1H, quin-Ar–H), 7.27–7.20 (m, 5H, Ar–H), 7.17–7.13 (m, 2H, Ar–H), 5.46 (s, 1H, = CH), 4.72 (s, 2H, benzylic-CH_2), 2.32 (s, 3H, CH_3).^{13}C NMR (101.0 MHz, DMSO-d_6) δ ppm 181.53, 162.32, 150.95, 138.97, 136.57, 131.00, 128.89, 127.52, 126.63, 126.11, 121.91, 114.85, 111.60, 93.01, 46.10, 20.16. GS MS: m/z calcd: 338.12, found: 338.39. Anal. Calcd for $C_{18}H_{18}N_4OS$ (324.10): C, 63.88; H, 5.36; N, 16.56. Found: C, 64.19; H, 5.20; N, 16.18.

***N*-Benzyl-2-(6-bromo-2-oxo-1,2-dihydroquinolin-4-yl) hydrazinecarbothioamide (6g)** Yield: 0.31 g (78%); mp: 243–245 °C, ^{1}H NMR (400 MHz, DMSO-d_6) δ ppm 11.20 (s, 1H, –CO–NH), 9.64 (s, 1H, $CH_2N\underline{H}$), 9.14 (s, 1H, quin-NH), 8.89 (s, 1H, NNH), 8.12 (s, 1H, quin-Ar–H), 7.64 (dd, J = 8.8, 1.1 Hz, 1H, quin-Ar–H), 7.29–7.23 (m, 4H, Ar–H),

7.21–7.19 (m, 2H, Ar–H), 5.48 (s, 1H, C = CH), 4.71 (s, 2H, benzylic-CH_2).^{13}C NMR (101.0 MHz, DMSO-d_6) δ ppm 181.10, 162.08, 150.16, 138.88, 137.67, 132.51, 127.54, 126.57, 126.14, 124.85, 117.00, 113.42, 112.02, 93.53, 46.09. GS MS: m/z calcd: 402.01, found: 402.47. Anal. Calcd for $C_{17}H_{15}BrN_4OS$ (402.01): C, 50.63; H, 3.75; N, 13.89. Found: C, 50.81; H, 3.67; N, 14.26.

***N*-Allyl-2-(2-oxo-1,2-dihydroquinolin-4-yl)hydrazinecarbothioamide (6h)** Yield: 0.22 g (79%); mp: 191–189 °C, ^{1}H NMR (400 MHz, DMSO-d_6) δ ppm 11.06 (s, 1H, –CO–NH), 9.55 (s, 1H, NNH), 9.07 (s, 1H, quin-NH), 8.46 (s, 1H, Allyl-NH), 7.90 (d, J = 8.0 Hz, 1H, Ar–H), 7.48 (t, J = 7.3 Hz, 1H, Ar–H), 7.28 (d, J = 8.0 Hz, 1H, Ar–H), 7.15 (dd, J = 7.8, 7.3 Hz, 1H, Ar–H), 5.82 (ddt, J_d = 17.4, 10.1 Hz, J_t = 5.1; 1H, CH_2 = Allyl), 5.43 (s, 1H, quin-C=CH), 5.07 (d, J = 17.2 Hz, 1H, CH = Allyl), 5.02 (d, J = 10.5 Hz, 1H, CH = Allyl), 4.09 (d, J = 4.6 Hz, 2H, CH_2-Allyl).^{13}C NMR (101.0 MHz, DMSO-d_6) δ ppm 181.10, 162.35, 151.09, 138.60, 134.58, 129.92, 122.28, 120.06, 114.90, 114.62, 111.70, 92.79, 45.19. GS MS: m/z calcd: 274.09, found: 274.80. Anal. Calcd for $C_{13}H_{14}N_4OS$ (274.09): C, 56.91; H, 5.14; N, 20.42. Found: C, 56.69; H, 5.38; N, 19.92.

***N*-Allyl-2-(6-methyl-2-oxo-1,2-dihydroquinolin-4-yl) hydrazinecarbothioamide (6i)** Yield: 0.25 g (87%); mp: 196–198 °C, ^{1}H NMR (400 MHz, DMSO-d_6) δ ppm 10.99 (s, 1H, –CO–NH), 9.53 (s, 1H, NNH), 8.97 (s, 1H, quin-NH), 8.43 (s, 1H, Allyl-NH), 7.72 (s, 1H, Ar–H), 7.31 (d, J = 7.2 Hz, 1H, Ar–H), 7.16 (d, J = 8.0 Hz, 1H, Ar–H), 5.81 (ddt, J_d = 17.0, 9.8, J_t = 5.0 Hz; 1H, Allyl = CH), 5.40 (s, 1H, quin-C=CH), 5.06 (d, J = 17 Hz, 1H, CH = Allyl), 5.01 (d, J = 11.0 Hz, 1H, CH = Allyl), 4.09 (d, J = 4.2 Hz, 2H, N-CH_2), 2.33 (s, 3H, CH_3).^{13}C NMR (101.0 MHz, DMSO-d_6) δ ppm 181.11, 162.27, 150.90, 136.56, 134.58, 130.92, 128.86, 121.92, 114.82, 114.62, 111.57, 92.92, 45.18, 20.16. GS MS: m/z calcd: 288.10, found: 288.26. Anal. Calcd for $C_{14}H_{16}N_4OS$ (288.10): C, 58.31; H, 5.59; N, 19.43. Found: C, 58.45; H, 5.21; N, 19.07.

***N*-Allyl-2-(6-bromo-2-oxo-1,2-dihydroquinolin-4-yl) hydrazinecarbothioamide (6j)** Yield: 0.28 g (80%); mp: 190–192 °C, ^{1}H NMR (400 MHz, DMSO-d_6) δ ppm 11.20 (s, 1H, –CO–NH), 9.56 (s, 1H, NNH), 9.10 (s, 1H, quin-NH), 8.52 (s, 1H, Allyl-NH), 8.13 (bs, 1H, Ar–H), 7.63 (d, J = 9.2 Hz, 1H, Ar–H), 7.21 (d, J = 8.4 Hz, 1H, Ar–H), 5.80 (ddt, J_d = 17.0, 10.5, J_t = 5.3 Hz; 1H, CH = Allyl), 5.42 (s, 1H, quin-C=CH), 5.06 (d, J = 18.0, 1H, CH = Allyl), 5.02 (d, J = 11.1 Hz, 1H, CH = Allyl), 4.08 (d, J = 5.0 Hz, 2H, CH_2-Allyl).^{13}C NMR (101.0 MHz, DMSO-d_6) δ ppm 181.05, 162.09, 150.16, 137.66, 134.52, 132.51, 124.90, 116.99, 114.65, 113.41, 112.02, 93.41, 45.20. GS MS: m/z calcd: 352.00, found: 352.69. Anal. Calcd for $C_{13}H_{13}BrN_4OS$ (352.00): C, 44.20; H, 3.71; N, 15.86. Found: C, 44.25; H, 3.42; N, 15.59.

Biology

Antifungal activity

Sabouraud agar (SA) media were prepared in the Mycological Center (AUMC), Assiut University, Assiut. The antifungal activity of tested compounds was determined according to the agar disk diffusion method [29]. *Rhodotorula mucilaginosa* AUMC 8795 was used to test the antifungal activity of the target compounds.

A suspension from spores in sterile distilled water was prepared: The spores were taken from 2- to 5-day-old culture of the test fungi growing on Sabouraud agar (SA) medium [29]. The final spore concentration was nearly 5×10^4 spores/mL. Approximately 15 mL of growth medium was then introduced on sterilized Petri dishes of 9 cm diameter and inoculated with 1 mL of spore suspension. Plates were shaken gently to homogenize the inocula. Antifungal activity of the tested compounds **6a–j** was performed by the standard agar disk diffusion method as follows:

Sterile 5-mM filter paper disk (Whatman) was saturated with 10 µL solutions of the test compound or clotrimazole (40 µmol/mL in DMSO). In addition, as a negative control, other disks were impregnated with the solvent (DMSO) and served. The disks were then dried for 1 h and placed in the center of each plate. The seeded plates were incubated at 28 ± 2 °C for 7 days. The radii of inhibition zones (in mM) of triplicate sets were measured at successive intervals during the incubation period, and the results are presented in Table 1.

Antibacterial activity and MIC determination

The antibacterial activity against *P. mirabilis* was tested using the cup-plate diffusion method [30]. Briefly, 0.5 ml of 1 × 108 CFU/ml (0.5 McFarland turbidity) *P. mirabilis* was plated in sterile Petri dish; then, 20 mL of Muller-Hinton agar (oxoid) was poured in the plates. After solidification of the media, four equidistant cups were made in the agar. Four different concentrations of the tested compounds were prepared by twofold serial dilutions in DEMSO; then, 100 µL of each concentration is applied to the cups separately. Compounds allowed diffusing into the Mullet-Hinton agar, and then, plates were incubated overnight at 35 °C. The inhibition zones of the bacteria around the cups were measured, and the MIC values were calculated by plotting the natural logarithm of the tested concentrations against squares of the

inhibition zone. The MIC value is the antilogarithm of the intercept on the logarithm of concentration axis.

Urease inhibitory activity In vitro screening and inhibitory studies on urease (Jack bean urease) were determined using colored Berthelot phenols method, which measures the liberation of ammonia from the reaction [40]. Briefly, the assay mixture, containing 1 unit of enzyme, was added to 650 µL of buffer solution (50 mMol phosphate buffer pH 6.7, 400 mMol sodium salicylate, 10 mMol sodium nitroprusside and 2 mMol EDTA/L) and mixed with 10 µL of different concentrations 0.1–100 mM of the tested compounds in DMF as a solvent. DMF was tested alone and showed no inhibitory effect on the enzyme. After 15 min of incubation at room temperature, 10 µL of 50 mg/L urea solution was add. The mixture was incubated for 0.5 h in water bath at 37 °C to allow the hydrolysis process.

After complete urea hydrolysis and ammonia liberation, the reaction was stopped by adding 200 µL of the hypochlorite reagent (150 mmol/L sodium hydroxide, 140 mm/L sodium hypochlorite). The ammonia liberated was allowed to complex with the hypochlorite and salicylate for 25 min at 30 °C. The absorbance was measured at 578 nm using UV/VIS Spectrophotometer (Optizen POP, 5U4608, Korea), and experiments were performed in triplicate in a final volume of 1 mL. All results were compared with thiourea, a standard inhibitor of urease. The percentage inhibition was calculated as the difference of absorbance values with and without the test compounds, and the concentration that provokes an inhibition halfway between the minimum and maximum responses of each compound (relative IC_{50}) was determined by monitoring the inhibition effect of various concentrations of compounds in the assay.

Molecular modeling

Molecular docking study The docking studies were performed using the OpenEye Modeling software [35–37]. A virtual library of target compounds was used, and their energies were minimized using the MMFF94 force field, followed by the generation of multi-conformers using the OMEGA application. The whole library of minimized energy values was docked appropriate target. The receptor PDB files were downloaded from the Protein Data Bank (PDB) (PDB ID: 3LA4) [38] and (PDB ID: 4UBP) [39]. Both the ligand input file and the receptor input file were passed into FRED to perform the molecular docking simulations. Multiple scoring functions were employed to predict energy profile of the ligand–receptor complex. The Vida application was employed as a visualization tool to show the ligands pose and the potential binding interactions of the ligands to the receptor of interest.

Shape alignment and ROCS The basic method to represent shape and color features in ROCS is using ROC application of OpenEye Scientific Software [35–37]. Compounds **I** and **II** [4] were selected as query molecules. Compounds library was adopted as the database file. Both query and database files were energy-minimized by Omega applications. ROCS runs were employed by personal PC in very fast using vROCS interface. vROCS was employed to run and analyze/visualize the results. ROCS application searched the database with the query to find molecules with similar shape and colors. Compound conformers were scored based upon the Gaussian overlap to the query, and the best-scoring parameters is Tanimoto Combo scores (shape + color); the highest score is best-matched with the query compound.

Acknowledgements Yaseen Elshaier acknowledges the OpenEye Scientific Software Inc. (Santa Fe, NM, USA) for providing the academic license that helped in performing the docking and ROCS studies. The NMR spectrometer at Florida Institute of Technology was purchased with the assistance of the US National Science Foundation (CHE 03 42251).

Compliance with ethical standards

Conflict of interest The authors declare that there is no conflict of interest regarding the publication of this article.

References

1. Prajapati SM, Patel KD, Vekariya RH, Panchal SN, Patel HD (2014) Recent advances in the synthesis of quinolines: a review. RSC Adv 4:24463–24476
2. Navneetha O, Deepthi K, Rao AM, Jyostna TS (2017) A review on chemotherapeutic activities of quinoline. Int J Pharm Chem Biol Sci 7:364–372
3. Saeed A, Zaib S, Pervez A, Mumtaz A, Shahid M, Iqbal J (2013) Synthesis, molecular docking studies, and in vitro screening of sulfanilamide-thiourea hybrids as antimicrobial and urease inhibitors. Med Chem Res 22:3653–3662
4. Ali B, Khan KM, Hussain S, Hussain S, Ashraf M, Riaz M, Wadood A, Perveen S (2018) Synthetic nicotinic/isonicotinic thiosemicarbazides: in vitro urease inhibitory activities and molecular docking studies. Bioorg Chem 79:34–45
5. Sen K, Komagata K (1979) Distribution of urease and extracellular DNase in yeast species. J Gener Appl Microbiol 25:127–135
6. Wirth F, Goldani LZ (2012) Epidemiology of Rhodotorula: an emerging pathogen. Interdiscip Perspect Infect Dis 2012:1–7
7. Burall LS, Harro JM, Li X, Lockatell CV, Himpsl SD, Hebel JR, Johnson DE, Mobley HL (2004) Proteus mirabilis genes that contribute to pathogenesis of urinary tract infection: identification of 25 signature-tagged mutants attenuated at least 100-fold. Infect Immun 72:2922–2938
8. Cernohorska L, Chvilova E (2011) Proteus mirabilis isolated from urine, resistance to antibiotics and biofilm formation. Klinicka mikrobiologie a infekcni lekarstvi 17:81–85
9. Tumbarello M, Trecarichi EM, Fiori B, Losito AR, D'Inzeo T, Campana L, Ruggeri A, Di Meco E, Liberto E, Fadda G (2012) Multidrug-resistant Proteus mirabilis bloodstream infections:

risk factors and outcomes. Antimicrob Agents Chemother 56:3224–3231
10. Singhal S, Arora S, Agarwal S, Sharma R, Singhal N (2013) A review on potential biological activities of thiosemicarbazides. World J Pharm Pharm Sci 2:4661–4681
11. Pitucha M, Karczmarzyk Z, Swatko-Ossor M, Wysocki W, Wos M, Chudzik K, Ginalska G, Fruzinski A (2019) Synthesis, in vitro screening and docking studies of new thiosemicarbazide derivatives as antitubercular agents. Molecules 24:251–267
12. Cihan-Üstündağ G, Gürsoy E, Naesens L, Ulusoy-Güzeldemirci N, Çapan G (2016) Synthesis and antiviral properties of novel indole-based thiosemicarbazides and 4-thiazolidinones. Bioorg Med Chem 24:240–246
13. Umadevi P, Deepti K, Srinath I, Vijayalakshmi G, Tarakaramji M (2012) Synthesis and in vitro antibacterial activity of some new urea, thiourea and thiosemicarbazide derivatives. Int J Pharm Pharm Sci 4:383
14. Wujec M, Kędzierska E, Kuśmierz E, Plech T, Wróbel A, Paneth A, Orzelska J, Fidecka S, Paneth P (2014) Pharmacological and structure-activity relationship evaluation of 4-aryl-1-diphenylacetyl (thio) semicarbazides. Molecules 19:4745–4759
15. Šarkanj B, Molnar M, Čačić M, Gille L (2013) 4-Methyl-7-hydroxycoumarin antifungal and antioxidant activity enhancement by substitution with thiosemicarbazide and thiazolidinone moieties. Food Chem 139:488–495
16. Masek BB, Merchant A, Matthew JB (1993) Molecular shape comparison of angiotensin II receptor antagonists. J Med Chem 36:1230–1238
17. Hawkins PC, Skillman AG, Nicholls A (2007) Comparison of shape-matching and docking as virtual screening tools. J Med Chem 50:74–82
18. Rush TS, Grant JA, Mosyak L, Nicholls A (2005) A shape-based 3-D scaffold hopping method and its application to a bacterial protein–protein interaction. J Med Chem 48:1489–1495
19. Khodair AI, Attia AM, Gendy EA, Elshaier YA, El-Magd MA (2019) Discovery of new S-glycosides and N-glycosides of pyridine-biphenyl system with antiviral activity and induction of apoptosis in MCF 7 cells. J Heterocycl Chem 56:1733–1747
20. Abdellatif KR, Fadaly WA, Kamel GM, Elshaier YA, El-Magd MA (2019) Design, synthesis, modeling studies and biological evaluation of thiazolidine derivatives containing pyrazole core as potential anti-diabetic PPAR-γ agonists and anti-inflammatory COX-2 selective inhibitors. Bioorg Chem 82:86–99
21. Adel MA, Ahmed IK, Eman AG, Mohammed AE-M, Yaseen AMME (2019) New 2-oxopyridine/2-thiopyridine derivatives tethered to a benzotriazole with cytotoxicity on MCF7 cell lines and with antiviral activities. Lett Drug Des Discov 16:1–14
22. Elbastawesy MAI, Aly AA, Ramadan M, Elshaier YAMM, Youssif BGM, Brown AB, Abuo-Rahma E-DAG (2019) Novel pyrazoloquinolin-2-ones: design, synthesis, docking studies, and biological evaluation as antiproliferative EGFR- TK inhibitors. Bioorg Chem 90:103045–103061
23. Abdullah MA, Abuo-Rahma GE-DA, Abdelhafez E-SM, Hassan HA, El-Baky RMA (2017) Design, synthesis, molecular docking, anti-Proteus mirabilis and urease inhibition of new fluoroquinolone carboxylic acid derivatives. Bioorg Chem 70:1–11
24. Abdullah MA, El-Baky RMA, Hassan HA, Abdelhafez E-SM, Abuo-Rahma GE-DA (2016) Fluoroquinolones as urease inhibitors: anti-Proteus mirabilis activity and molecular docking studies. Am J Microbiol Res 4:81–84
25. Toolkit, OEChem (2012) OpenEye Scientific Software, Santa Fe, NM, (USA)
26. Abass M (2000) Chemistry of substituted quinolinones. Part II synthesis of novel 4-pyrazolylquinolinone derivatives. Synth Commun 30:2735–2757
27. Ismail M, Abass M, Hassan M (2000) Chemistry of substituted quinolinones. Part VI. Synthesis and nucleophilic reactions of 4-chloro-8-methylquinolin-2 (1H)-one and its thione analogue. Molecules 5:1224–1239
28. Ismail M, Abdel-Megid M, Hassan M (2004) Some reactions of 2-and 4-substituted 8-methylquinolin-2 (1H)-ones and their thio analogues. Chem P-Slovak Acad Sci 58:117–125
29. William H (1977) Microbiological assay. An introduction to quantitative principles and evaluation. Academic Press, New York
30. Miller RE, Rose SB (1941) Studies with the agar cup-plate method: IV. A correlation of agar cup-plate data with antiseptic dilution data. Am J Clin Pathol 11:414–424
31. Pervez H, Iqbal MS, Tahir MY, F-u-H Nasim, Choudhary MI, Khan KM (2008) In vitro cytotoxic, antibacterial, antifungal and urease inhibitory activities of some N 4-substituted isatin-3-thiosemicarbazones. J Enzyme Inhib Med Chem 23:848–854
32. Schulz M, Iwersen-Bergmann S, Andresen H, Schmoldt A (2012) Therapeutic and toxic blood concentrations of nearly 1000 drugs and other xenobiotics. Crit Care 16:136–140
33. Sujoy B, Aparna A (2013) Potential clinical significance of urease enzyme. Eur Sci J 9:94–102
34. Mobley H, Island MD, Hausinger RP (1995) Molecular biology of microbial ureases. Microbiol Mol Biol Rev 59:451–480
35. Fast Rigid Exhaustive Docking (FRED) Receptor, version 2.2.5; OpenEye Scientific Software, Santa Fe, NM (USA); http://www.eyesopen.com
36. OMEGA, version 2.5.1.4; OpenEye Scientific Software, Santa Fe, NM (USA); http://www.eyesopen.com
37. VIDA, version 4.1.2; OpenEye Scientific Software, Santa Fe, NM (USA); http://www.eyesopen.com
38. Balasubramanian A, Ponnuraj K (2010) Crystal structure of the first plant urease from jack bean: 83 years of journey from its first crystal to molecular structure. J Mol Biol 400:274–283
39. Benini S, Rypniewski WR, Wilson KS, Miletti S, Ciurli S, Mangani S (2000) The complex of Bacillus pasteurii urease with acetohydroxamate anion from X-ray data at 1.55 Å resolution. J Biol Inorg Chem 5:110–118
40. Weatherburn M (1967) Phenol-hypochlorite reaction for determination of ammonia. Anal Chem 39:971–974